




Bitemporal analysis of burned areas in the Atlantic Forest

*Iorrana Figueiredo Sacramento*¹ 
*Roberto Ferreira Machado Michel*² 
*Rafael Gomes Siqueira*³ 

Keywords:

Image classification
Image segmentation
Band ratio
Variables selection;
Forest fire.

Abstract

The study of burned areas is used as a subsidy for fire control and monitoring in the protected areas. In face of the challenges of the spectral signature characterization of burned areas, this study aimed to apply the object-oriented classification method and to evaluate the performance of spectral indices subsets for mapping burned areas in the Atlantic Forest. For that, we performed a bitemporal analysis between 2014 and 2016, considering the difference of each spectral indices among two LANDSAT 8 images: pre-and post-fire. The object-oriented classification was performed automatically by segmentation, supervised classification and optimization algorithms in the GIS environment. The “weak” burn severity class was the most expressive, with 13.65% of the mapped area, while the “severe” burn severity class occupied 0.3%. The burned areas presented an increase of reflectance in the red and shortwave infrared bands and a decrease in the near infrared band. The Δ NBR was the best discriminator of burned area and the Δ NBR, Δ NBR2, Δ NDMI, Δ SAVI, Δ NDVI, Δ GEMI and Δ MSAVI set presented the highest separation threshold. The validation of the classification by the Kappa agreement coefficient obtained a good outcome (0.72). The selection of the variables showed efficiency in determining the spectral indices’ subset with the best performance for detecting the classes of burned areas, improving the classification accuracy and reliability. The segmentation was also important for the effectiveness of the object-oriented classification, being directly influenced by the image spatial resolution.

¹Programa de Pós-Graduação em Solos e Nutrição de Plantas – UFV. iorranafigueiredos@gmail.com

² Departamento de Ciências Agrárias e Ambientais – UESC. roberto@michel.com

³Programa de Pós-Graduação em Solos e Nutrição de Plantas – UFV. rafael.geo.siqueira@gmail.com

INTRODUCTION

The Atlantic Forest (AF) is a biome historically threatened by the anthropic pressure and it is considered a worldwide hotspot that presents altered and fragmented areas (PINTO et al., 2006). Between 1986 and 2001, although the AF has increased 5% of its absolute cover in the South of Bahia (BA), Brazil, there was an intense fragmentation of the landscape, with an increase in the number of fragments smaller than one hundred hectares (SAVE BRASIL; IESC; BIRDLIFE INTERNATIONAL, 2009). Studies in the Biological Reserve of Una – BA (REBIO of Una) showed a great quantity of *cabruças* (agroforestry systems where the cocoa trees are planted under the forest shadows) and secondary forests, which contribute to decrease the isolation and maintain the populations of animals and plants in the region. This fact emphasizes the importance of maintaining contiguous areas of protected areas.

The burned areas represent a recurrent threat for the protected areas (SANTOS; SOARES; BATISTA, 2006; 2018). The use of fire for soil management has a millenary nature (BENTO-GONÇALVES et al., 2012; CHUVIECO, 1997; MISTRY; BIZERRIL, 2011). The traditional management is the main agricultural strategy in the Wildlife Refuge of Una – BA (REVIS of Una) (SOLLBERG; SCHIAVETTI; MORAES, 2014) and, despite this technique embraces conservationists' practices, it also uses slash-and-burn agriculture. The fire consequences affect the forests' composition and structure, the animal biodiversity, the human health and the atmospheric balance, both on a local and regional scale (COCHRANE, 2003; DODONOV et al., 2019; FREITAS et al., 2005; MENEZES; CAZETTA; DODONOV, 2019).

The creation of fire prevention and monitoring politics has become possible through the application of remote sensing techniques, once they allow extracting information quickly and efficiently, which are used for burned areas identification, control and supervision (CHUVIECO, 1996; DOS SANTOS et al., 2018; FREITAS et al., 2005; PEREIRA, 2009; SANTOS et al., 2020). The bitemporal analysis of satellite images has been widely used for detecting and monitoring environmental

changes, mainly for the estimation of burned areas and the detection of fire severity (CARDOZO et al., 2011; CARVAJAL-RAMIREZ et al., 2019; ESCUÍN; NAVARRO; FERNÁNDEZ, 2008; SANTOS et al. 2020). The object-oriented classification is a valuable method for considering not just the spectral information, but also the spatial relationships as shape and context. As consequence, the outcome is a more sophisticated classification and closer to human interpretation, without the common “salt and pepper” effect of the pixel-by-pixel method (McDERMID, et al., 2003; WONG et al., 2003).

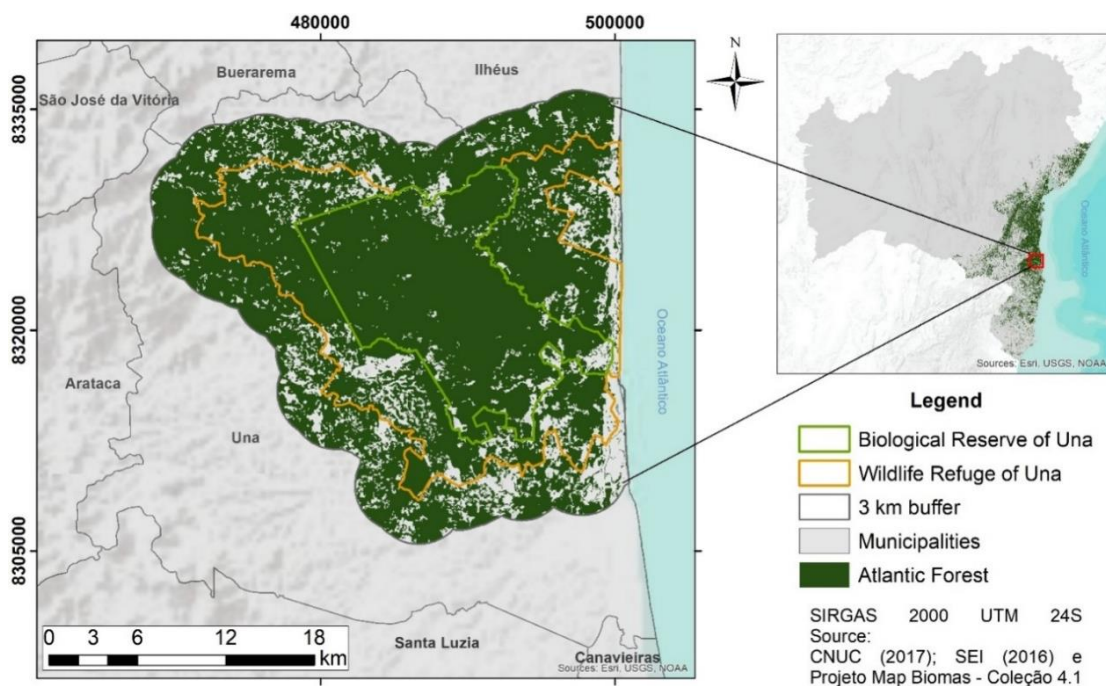
However, burned areas detection using remote sensing is limited due to the difficulty to discriminate fire from possible imaging failures, that can restrict the detection (COCHRANE, 2003). Besides, the confusion tendency between burned areas and other land uses has led to the need for a better characterization of the spectral signature of burned areas, which has been possible through spectral indices. These indices help discriminating land surface targets, through arithmetic calculation with spectral bands (CARVAJAL-RAMIREZ et al., 2019; DOS SANTOS et al., 2018; LEITE et al., 2017; SANTOS et al., 2020). Therefore, the main goals of this research were to apply the object-oriented classification method and to evaluate the best performance of sets of spectral indices' for mapping burned areas in the AF of South of Bahia.

MATERIALS AND METHODS

Study area

The study area (709.7 km²) comprises the protected areas of integral protection: REBIO of Una (187 km²), REVIS of Una (232 km²) and their surrounding areas (a radius of 3 km). These units were created in 1980 and 2007, respectively (BRASIL, 1980; 2007). The study area is in the municipality of Una, South of Bahia's region (Figure 1). The estimated population of Una is 19.000 inhabitants and its demographic density is 16.86 inhabitants per km² (IBGE, 2019). Its economy is mainly based on agriculture and extractivism, highlighting the cocoa production (*cabruças*), rubber agriculture, coffee, manioc, coconut, açaí palm and banana (IBGE, 2017).

Figure 1 – Location map of REBIO of Una, REVIS of Una and their surroundings, and the AF extension in the study area in 2018.

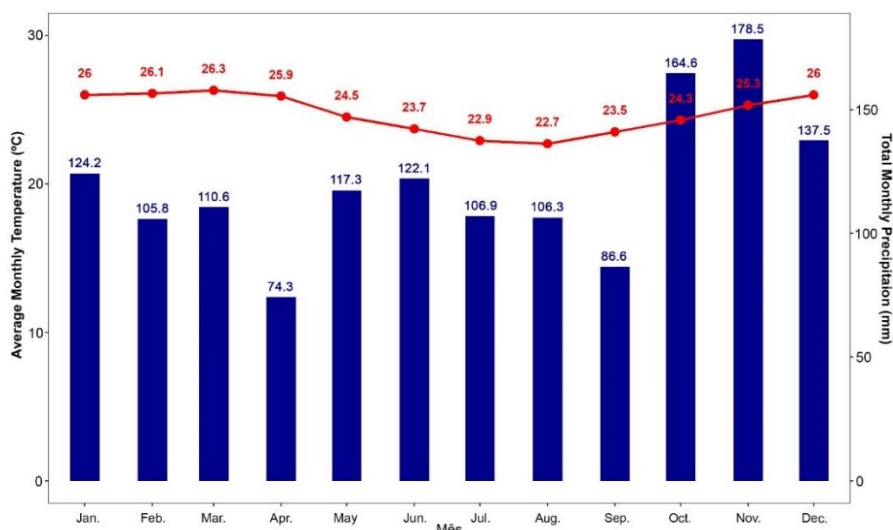


Source: MAPBIOMAS (2020). Org.: by the authors, 2020.

The study area integrates the Serra das Lontras Complex, formed by three connected mountains that are part of the Serras e Maciços Pré-Litorâneos geomorphological unit (SAVE BRASIL; IESB; BIRDLIFE INTERNATIONAL, 2009). The region is characterized by well-distributed rains over the year, with annual precipitation around 1,400 mm and annual mean temperature of 24.8 °C (Figure 2). The air relative humidity was 84% in 2014 (INMET, 2020). These conditions provide the formation of

deep, well-drained and porous soils - Yellow and Yellow-Red Latosols - originated from crystalline rocks (SAVE BRASIL; IESB; BIRDLIFE INTERNATIONAL, 2009). The Dense Ombrophilous Forest currently corresponds to 81% of the study area (Figure 1) and had increased about 1% since 1988 (MAPBIOMAS, 2020), evidencing the importance of the protected areas for the conservation of the AF remaining fragments.

Figure 2 – The average of the monthly temperature and the average of the total monthly precipitation, between 2012 and 2016 in Una – Bahia.



Source: INMET (2020). Org.: by the authors, 2020.

Materials

We used the 30 meters spectral resolution bands of the Operational Land Imager Sensor - OLI, LANDSAT 8 (path/row 215/71) (Table 1). These products were obtained post-processed, with geometric and surface reflectance corrections – atmospheric absorption or scattering correction (BARSİ et al., 2014; VERMOTE et al., 2016). The 15 meters panchromatic band was only used for the segmentation step to enhance the detailing. The pre-fire image was from August 7th, 2014 and the post-fire image was from April 6th, 2016. We selected images from different periods due to the lower cloud cover and to the

absence of a marked dried period in the region (Figure 2), which ensured similar spectral response of the vegetation over the year.

We obtained the hot spots data from the Banco de Dados de Queimadas (BDQ) of the Instituto Nacional de Pesquisas Espaciais (INPE, 2018), the Brazilian spatial institute. These data were generated by polar satellite images NOAA and EOS, and geostationary satellite images GOES and METESAT. Between 2014 and 2016, 224 hot spots were identified in the study area. These information were used as evidence of fire occurrence and were applied in the classification's validation step.

Table 1. Spectral bands of LANDSAT 8.

Band	Name	Range (nm)
1	Ultra blue	435 – 451
2	Blue (B)	452 – 512.1
3	Green (G)	532,7 – 590.1
4	Red(R)	635.9 – 673.3
5	Near Infrared (NIR)	850.5 – 878.8
6	Shortwave Infrared 1 (SWIR 1)	1,566.5 – 1,651.2
7	Shortwave Infrared 2 (SWIR 2)	2,107.4 – 2,294.1
8	Panchromatic (PAN)	503.3 – 676.7

Source: USGS (2018). Org.: by the authors, 2020.

Object-oriented classification

We performed the processing in eCognition 9 software. For the classification, the clouds, shadows, and water bodies from the pre-and post-fire images were removed. From the post-fire image, we created five classes of change detection: 1 – severe, 2 – moderate, 3 – weak (burn severity classes), 4 – no alteration class, and 5 – regeneration class (change occurred by biomass increasing). Burn severity classes followed the criteria: the sever class corresponded to the burned areas' epicenter, the "weak" class is the edge zones, and the "moderate" class is the transition between "severe" and "weak" classes. For each class, we collected 15 training samples, totalizing 75 samples.

All bands from the post-fire image were used in the segmentation step. We applied the Multiresolution Segmentation algorithm (BAATZ; SHÄPE, 2000). This algorithm

initiates the segmentation with each image pixel representing one object, which can be grouped to a neighbor pixel according to the scale and homogeneity parameters. The first parameter defines the maximum heterogeneity allowed in an object and it influences its size. The second refers to a color and geometry relationship of the objects aiming to create objects as less heterogeneous as possible (DEFINIENS, 2012). We made tests to define these parameters and the values of scale 80, shape 0.2 and compactness 0.5 showed more suitability for the study area.

Then, we calculated the following spectral indices through the bands ratio, for the pre-and post-fire images: Normalized Difference Vegetation Index – NDVI (Equation 1) (ROUSE et al., 1973); Enhanced Vegetation Index – EVI (Equation 2) (JENSEN, 2009); Soil Adjusted Vegetation Index – SAVI (Equation 3) (HUETE, 1988); Modified Soil Adjusted Vegetation Index – MSAVI (Equation 4) (QI et al., 1994);

Normalized Difference Moisture Index – NDMI (Equation 5) (JESEN, 2009); Normalized Burnt Ratio – NBR (Equation 6) (KEY; BENSON, 1999); Normalized Burnt Ratio 2– NBR2 (Equation 7) (MARTÍN; GÓMEZ; CHUVIECO, 2005); Burned Area Index – BAI (Equation 8) (CHUVIECO; MARTÍN; PALACIOS, 2002); Global Environmental Monitoring Index – GEMI (Equation 9a e 9b) (PINTY; VERSTRAETE, 1992).

$$NDVI = \frac{(NIR-R)}{(NIR+R)} \quad (\text{Equation 1})$$

$$EVI = G * \left(\frac{(NIR-R)}{(NIR+C1R-C2B+L)} \right) \quad (\text{Equation 2})$$

$$SAVI = \left(\frac{(NIR-R)}{(NIR+R+L)} \right) * (1+L) \quad (\text{Equation 3})$$

$$MSAVI = \frac{(2NIR+1 - \sqrt{((2NIR+1)^2 - 8*(NIR-R))})}{2} \quad (\text{Equation 4})$$

$$NDMI = \frac{(NIR-SWIR1)}{(NIR+SWIR1)} \quad (\text{Equation 5})$$

$$NBR = \frac{(NIR-SWIR2)}{(NIR+SWIR2)} \quad (\text{Equation 6})$$

$$NBR2 = \frac{(SWIR1-SWIR2)}{(SWIR1+SWIR2)} \quad (\text{Equation 7})$$

$$BAI = \frac{1}{((0.1-R)^2) + ((0.6-NIR)^2)} \quad (\text{Equation 8})$$

$$GEMI = \frac{\eta * (1 - 0.25 * \eta) - (RED - 0.125)}{(1 - RED)} \quad (\text{Equation 9a})$$

At which:

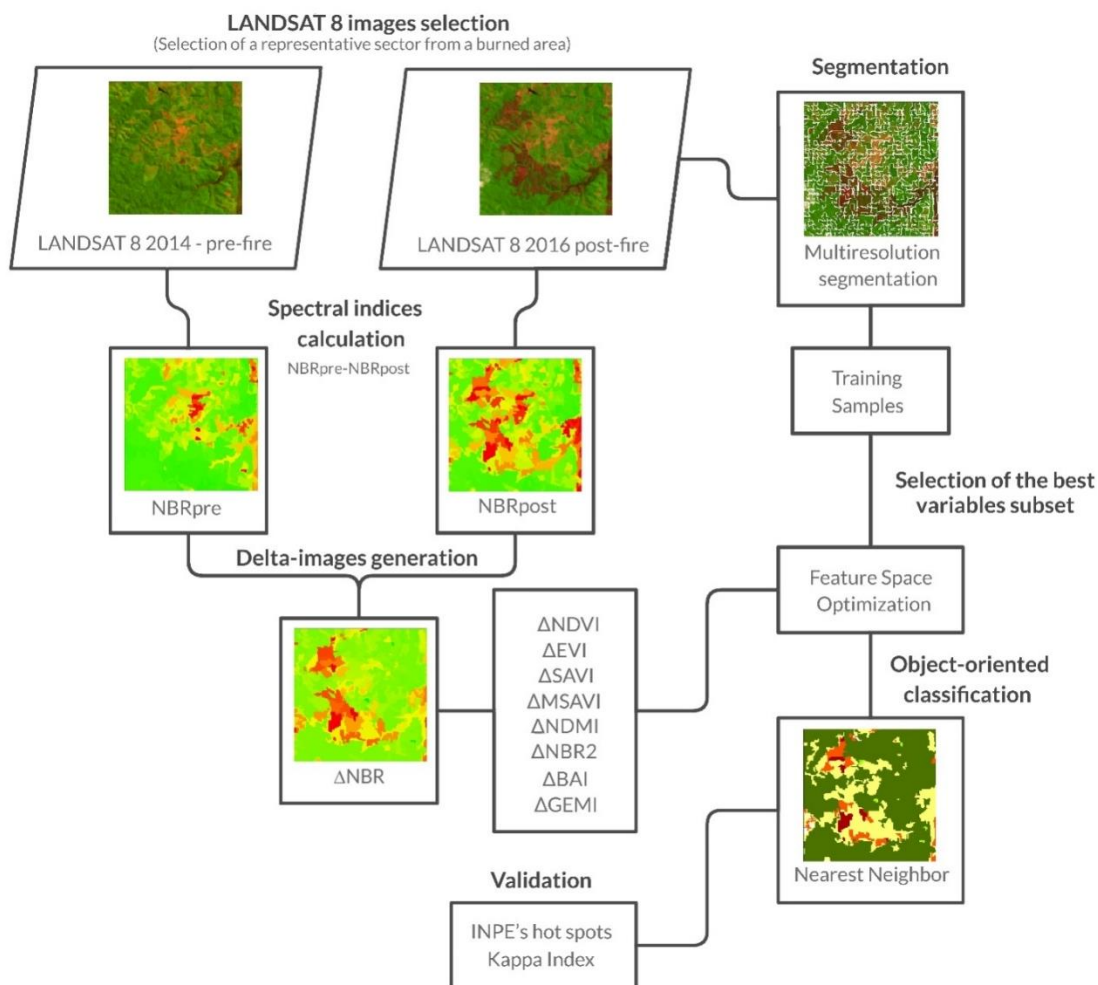
$$\eta = \frac{(2 * (NIR^2 - RED^2) + 1.5 * NIR + 0.5 * RED)}{(NIR + RED + 0.5)} \quad (\text{Equação 9b})$$

Then, we calculated the delta-images, that correspond to the difference between the pre-fire and post-fire indices images (Δ indices = pre-fire index – post-fire index). As a result, the delta-images areas where the vegetation suppressed obtained values > 0 ; where there was regeneration, the values were < 0 ; and where there was no change, the values were close to 0 (CARDOZO et al., 2011; PEREIRA, 2009).

Next, we used the Feature Space Optimization tool to define which delta-images were more suitable for the classification. This tool ranks the variables (delta-images) by importance order and creates a number of different size subgroups (dimensions), proportional to the number of the cumulative variables (dim 1 = one variable; dim 2 = two variables, dim 3 = three variables... dim n = n variables). For each dimension, the algorithm calculates the Euclidean distance (from 0 to 1) between the objects of each mapped class, in order to find the variable combination that presents the greater distance and, consequently, the greater classes separation threshold (TRIMBLE, 2014).

From this, we performed the supervised classification through the Nearest Neighbor algorithm. This algorithm works considering the distance between the object to be classified and the nearest training sample, in other words, as the closer is the object of a sample, the greater the relationship between them (GABRIEL, 2013), and then it is grouped to the sample's class. The Nearest Neighbor was the algorithm with the best performance among the object-oriented classifiers tested by Zanotta et al. (2010).

For the validation step, we applied the Kappa index considered, in many works, as appropriate to measure a classification accuracy (GABRIEL, 2013). This index was applied through the Assessment Accuracy tool and for that, we collected 65 samples based on the INPE's hot spots. According to Landis e Koch (1977), the Kappa index values range from 0 to 1, being 0 – 0.2 = bad; 0.2 – 0.4 = reasonable; 0.4 – 0.6 = good; 0.6 – 0.8 = very good; and 0.8 – 1.0 = excellent. The whole processing is briefly presented below (Figure 3).

Figure3 – The object-oriented classification method steps.

Source: The authors, 2020.

RESULTS AND DISCUSSION

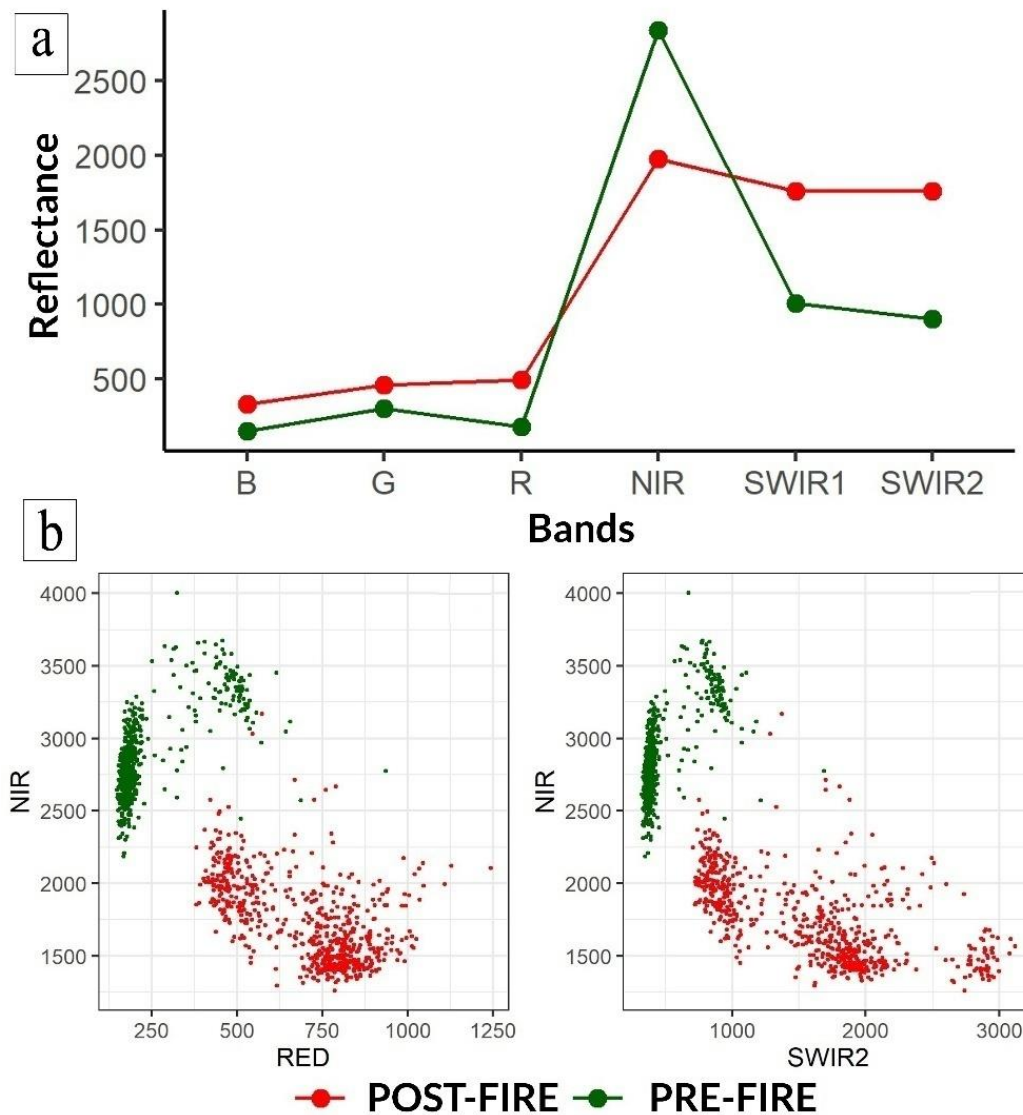
Figure 4a shows the average reflectance values of samples of burned areas for the pre-and post-fire spectral bands. There was an increase of the reflectance at the visible region (RGB) and at the mid-infrared (SWIR1 and SWIR2), with higher alteration in the visible at the red (R) band. In the pre-fire image, with greater biomass condition, the reflectance at the R was less than the green (G) band, and the inverted situation happened in the post-fire image.

On the other hand, the near-infrared band (NIR) had a significant reflectance decrease (MARTÍN; CHUVIECO; 1998). This led to a decrease in the difference between the NIR and R bands, and between the NIR and SWIR bands, which affected directly the spectral indices behavior. Figure 4b shows the reflectance pixel

values of burned areas for the R, NIR and SWIR2 bands. The reflectance values of the burned areas at the R and SWIR2 bands were higher in the post-fire image, while the values of the NIR band were higher in the pre-fire image.

The reflectance increase in the visible region, as well as the reflectance increase at the R band compared with the G band, is explained by the decrease of the radiation absorption of the photosynthetic pigments, due to the biomass loss caused by the burning (PONZONI; SHIMABUKURO, 2007). Despite this difference, the visible region is not indicated for burned areas discrimination, due to its low reflectance and to the atmospheric scattering influence, mainly over dark surfaces, as burned areas, which decreases the contrast between the surface targets (PEREIRA et al., 1999).

Figure 4 – a) Reflectance average of the burned areas at the pre and post-fire images; b) Reflectance of burned area pixels for R, NIR and SWIR2 bands.

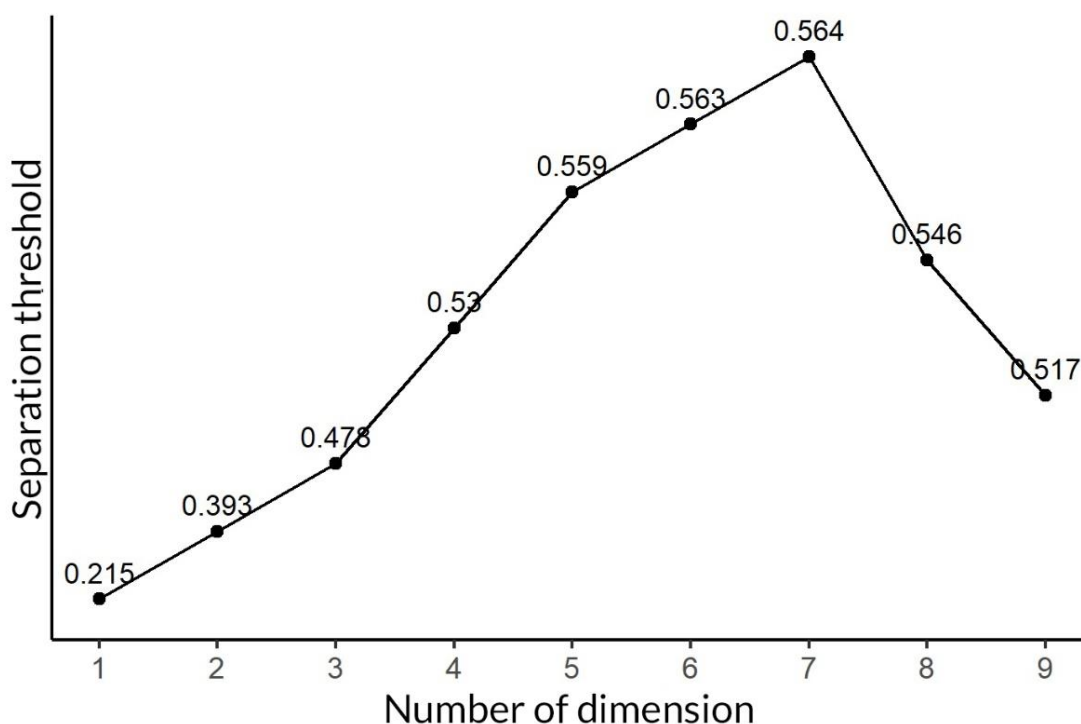


Source: The authors, 2020.

The NIR reflectance decrease (around 30%) can be explained by the plant cell structure destruction during the burning. Due to the great reflectance difference of the NIR in the pre-and post-fire images, this band was highlighted as the best one for burned areas discrimination (PEREIRA et al., 1999). The significant increase of the reflectance values for the SWIR1 and SWIR2 bands (75.4% and 94.7%, respectively) is due to the decrease of the leaf water content (MARTÍN; CHUVIECO, 1998). The mid-infrared region was recognized as effective to the distinction of burned areas, due to its high reflectance and to the minimum atmospheric scattering influence (PEREIRA et al., 1999).

The Feature Space Optimization algorithm

was efficient in the selection of the more suitable delta-images for classification (Figure 5 and Table 2). Considering just one delta-image in the analysis (dimension 1), the ΔNBR was the one with the greater capacity of change detection classes discrimination. However, the biggest separation threshold (0.564) was found when considering seven from nine calculated indices (dimension 7). From dimension 7, the high number of delta-images induced redundancies, which decreased the classes separation threshold. The Feature Space Optimization algorithm efficiency to enhance image classification performance was already highlighted in earlier studies (DURRIEU et al., 2007; LEDUC, 2004).

Figure 5 – Representation of the separation thresholds for each analyzed dimension.

Source: The authors, 2020.

Table 2. Analysis dimensions and its respective separation thresholds.

Dimensio n	Delta-image	Threshold
1 ^a	Δ NBR	0.215
2 ^a	Δ NBR and Δ NBR2	0.393
3 ^a	Δ NBR, Δ NBR2 and Δ NDMI	0.478
4 ^a	Δ NBR, Δ NBR 2, Δ NDMI and Δ SAVI	0.530
5 ^a	Δ NBR, Δ NBR 2, Δ NDMI, Δ SAVI and Δ NDVI	0.559
6 ^a	Δ NBR, Δ NBR 2, Δ NDMI, Δ SAVI, Δ NDVI and Δ GEMI	0.563
7 ^a	Δ NBR, Δ NBR 2, Δ NDMI, Δ SAVI, Δ NDVI, Δ GEMI and Δ MSAVI	0.564
8 ^a	Δ NBR, Δ NBR 2, Δ NDMI, Δ SAVI, Δ NDVI, Δ GEMI, Δ MSAVI and Δ BAI	0.546
9 ^a	Δ NBR, Δ NBR 2, Δ NDMI, Δ SAVI, Δ NDVI, Δ GEMI, Δ MSAVI, Δ BAI and Δ EVI	0.517

Source: The authors, 2020.

The NBR and NBR2 burned area indices were the most significant in this study and the ones that also discriminate better the burned areas according to earlier studies (CARDOZO et al., 2011; ESCUÍN; NAVARRO; FERNÁNDEZ, 2008; PEREIRA, et al., 2015; ROSAN; ALCÁNTARA, 2015). This is because the bands used in their calculation (NIR and SWIR2) are the ones that suffered the most significant post-fire spectral alterations. The Δ NDMI was the third-best delta-image for discriminating the change detection classes of burned areas. The NDMI humidity index also showed greater potential for burning detection than the

vegetation indices according to Wilson and Sader (2002), which is due to the changes of soil and plant humidity regime after burning.

Among the vegetation indices, the SAVI had the greatest capacity of burning detection and it also presented moderate performance according to Pereira et al. (2015). The MSAVI is similar to SAVI, although the last one uses a soil effect correction factor manually adjusted according to the environmental conditions of each area and the first one uses an auto-adjusted factor (Qi et al., 1994), whose hardness can induce to poor results comparing to SAVI, as verified in this research. In this study, the NDVI did not

present great efficacy for burned areas detection, although it is widely applied (CARDOZO et al., 2011; ESCUÍN; NAVARRO; FERNÁNDEZ, 2008; PEREIRA, 1999; PEREIRA, et al., 2015). The GEMI proved to be better than NDVI for burned areas detection since it is less affected by atmospheric and soil influence (PEREIRA, 1999). Herein, the performance differences between the NDVI and GEMI delta-images were not significant, and both of them showed a moderate performance. The BAI did not contribute to the class separability enhance, it is considered a good burned area detection index though (CHUVIECO; MARTÍN, PALACIOS, 2002; DEMPWOLF, et al., 2007). As the BAI, the EVI did not contribute to the increase of the burned areas' differentiation and presented a low separability according to Pereira et al. (2015).

According to the Euclidian distance matrix between the change detection classes (Table 3), the “no alteration” and “regeneration” classes presented the lowest separation value (0.56), once they correspond to vegetated areas and therefore, they had similar spectral responses. The “severe” burned class presented the highest separability values with the two previous classes (28.6 and 37.7, respectively) due to the great biomass loss associated with the burning. Among the burning severity classes (classes 1, 2 and 3), the “severe” and “moderate” classes showed the lowest separation value (0.9) and the “severe” and “weak” classes showed the biggest one (4.7). Comparing the distances between the burned area classes and the others, the “weak” and “no alteration” classes presented the smallest separation value (5.3).

Table 3. Euclidean distance matrix presenting the separation value by class: 1 – severe; 2 – moderate, 3 – weak; 4 – no alteration; and 5 – regeneration.

Classes	1	2	3	4	5
1	0	0.9	4.7	28.6	37.7
2	0.9	0	1.4	17.3	24.6
3	4.7	1.4	0	5.3	9.4
4	28.6	17.3	5.3	0	0.6
5	37.7	24.6	9.4	0.6	0

Source: The author, 2020.

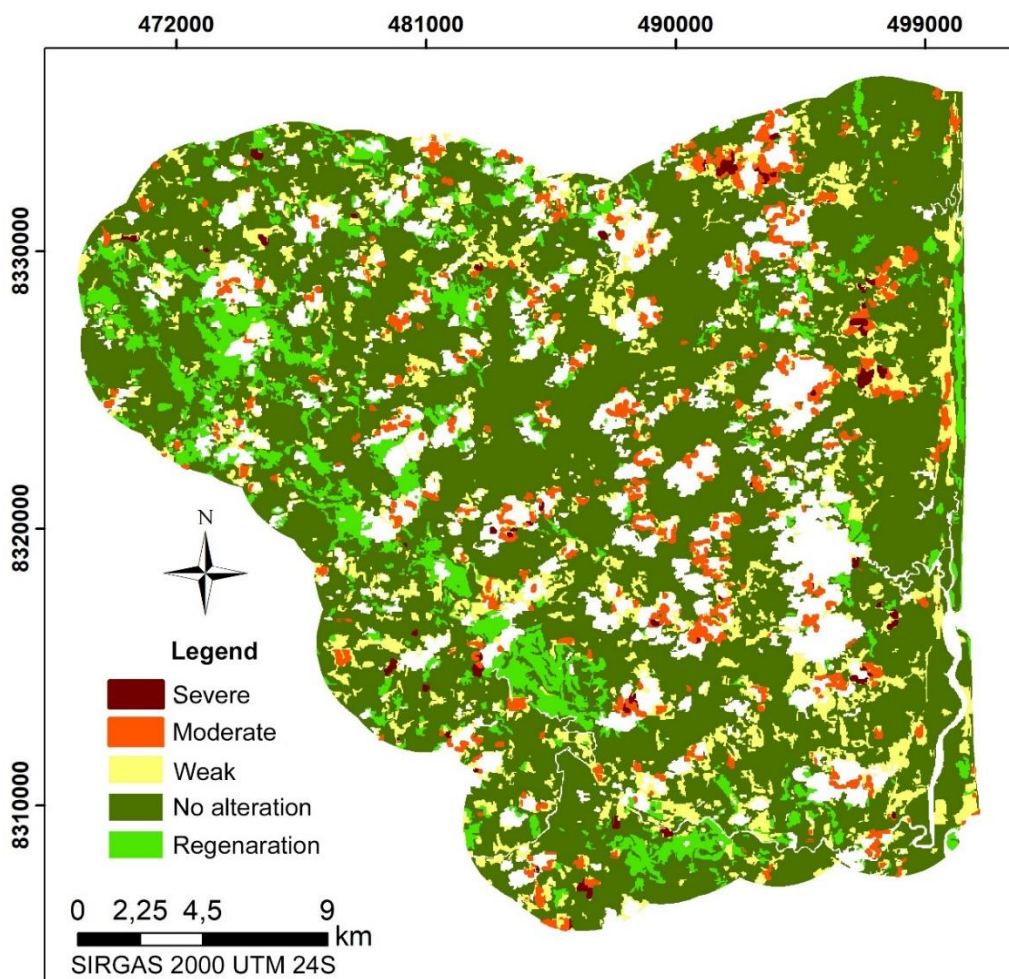
The “weak” severity class corresponds mainly to the burned areas edge, where the spectral difference between the pre-and-post-fire images was smaller, and the “severe” class corresponds to the burning epicenter, where the changes induced by the fire were bigger. The proximity between the distance values of the “weak” class with the “severe” and “no alteration” classes indicates a transitional condition of the “weak” class in the study area.

According to the final classification, around 74% of the total area did not pass through significant changes in the vegetation cover during the analyzed period (Figure 6 and Table 4). The burned area classes represent 16.1% of the mapped area and they were more pronounced in the northeast sector, which corresponds to the REVIS of Una and its surroundings (Figure 6), a sector where the land

use is allowed and more intense. From this percentage, 13.65% corresponds to the “weak” class, while 0.3% corresponds to the “severe” class (Table 4).

Nevertheless, we also observed an overestimation of the “weak” class. The overestimation could have occurred for three reasons: occurrence of areas where the change was less noticed, with positive values of delta-images next to 0, as in the coastal areas; areas around clouds, whose influence resulted in positive values next to 1; or where there was a confusion generated by the presence of misclassified pixels inside some objects. This can be associated with the low spatial resolution of the LANDSAT8 images, that interfered in the segmentation process, once unburned pixels were included inside some burned area classes, mainly the “weak” class.

Figure 6 – Object-oriented classification of the study area.



Source: The authors, 2020.

Table 4 – Quantification of the burned and vegetated areas of the study area.

Classes	Area (km ²)	Area (%)
Severe	1.9	0.3
Moderate	12.7	2.15
Weak	80.7	13.65
No alteration	436.5	73.82
Regeneration	59.6	10.08
Total	591.3	100

Source: The authors, 2020.

From the total mapped burned areas (95.23 km²), 45% were identified in the surrounding area; 34% in the REVIS of Una; and 21% in the REBIO of Una, indicating the best effectivity of the last one in preventing fires. The classification Kappa value was 0.72, corresponding to a very good classification according to Landis e Koch (1977).

CONCLUSION

The use of delta-images from pre-and post-fire spectral indices showed efficiency to the land cover change detection through burnings in the Atlantic Forest in the South of Bahia. With the variable’s selection using the Feature Space

Optimization algorithm, we identified the most suitable spectral indices' subset to enhance the object-oriented classification accuracy. The NBR delta-image showed the best performance, while the seven spectral indices' subset presented the greater separation threshold, embracing a combination of burning, humidity and vegetation indices.

Our results showed that the integrated use of different spectral indices potentializes the classifier performance when compared to the use of the indices particularly. However, we observed that the performance increase is not directly proportional to the variables increase, once the use of more than seven indices increased the information's confusion and redundancy, which contributed to reduce the separability level between classes.

The object-oriented classification also showed strong dependency of the segmentation step, once the classification is directly applied over the segmentation's created objects, which shall involve as precisely as possible the pixels correspondent to the same surface target. The medium to low spatial resolution of the LANDSAT8 images induced a certain spectral confusion among the evaluated classes. An alternative to obtain more homogeneous objects in limited spatial resolution images would be the use of the spectral mixing method, that permits the identification of the different target's influence (vegetation, soil, shadow, e.g.) in a burned area pixel.

REFERENCES

- BARSI, J. A. et al. The spectral response of the Landsat-8 Operational Land Imager, **Remote Sensing**, v. 6, p. 10232-10251, 2014. <https://doi.org/10.3390/rs61010232>
- BAATZ, M.; SCHÄPE, A. Multiresolution segmentation: an optimization approach for high quality multi-scale image segmentation. In: STROBL; BLASCHLE; GRIESEBNER (Org.) **Angewandte Geographische Informationsverarbeitung XII**, Heidelberg: Wichmann-Verlag, 2000.
- BENTO-GONÇALVES, A. et al. Fire and soils: Key concepts and recent advances. **Geoderma**, v. 191, p. 3-13, 2012. <https://doi.org/10.1016/j.geoderma.2012.01.004>
- BRASIL. **Decreto Federal n. 85.463, de 10 de dezembro de 1980**. Available in: <http://www.planalto.gov.br/ccivil_03/atos/decretos/1980/D85463.html>. Accessed: August 13, 2020.
- BRASIL. **Decreto Federal s/n., de 21 de dezembro de 2007**. Available in: <http://www.planalto.gov.br/ccivil_03/_ato2007-2010/2007/dnn/Dnn11459.htm>. Accessed: August 13, 2020.
- CARDOZO, F. S. et al. Avaliação de áreas queimadas a partir dos índices espectrais NDVI e NDBR. In: Simpósio Brasileiro de Sensoriamento Remoto, 15., 2011, **Anais...** Curitiba, 2011. p. 7950-7957. Available in: <<http://marte.sid.inpe.br/col/dpi.inpe.br/marte/2011/07.27.21.58/doc/p1429.pdf>>. Accessed: April 10, 2018.
- CARVAJAL-RAMIREZ, F. et al. Evaluation of Fire Severity Indices Based on Pre- and Post-Fire Multispectral Imagery Sensed from UAV. **Remote Sensing**, v. 11, n. 993, p. 1-19, 2019. <https://doi.org/10.3390/rs11090993>
- CHUVIECO, E. (Ed.). **A review of remote sensing methods for the study of large wildland fires**. Spain: Universidad de Alcalá, 1997. 192 p.
- CHUVIECO, E. Empleo de imágenes de satélite para medir la estructura del paisaje: análisis cuantitativo y representación cartográfica. **Serie Geográfica**, v. 6, p. 131-147, 1996. Available in: <<https://core.ac.uk/download/pdf/58902321.pdf>>. Accessed: April 20, 2018.
- CHUVIECO, E.; MARTÍN, M. P.; PALACIOS, A. Assessment of different spectral indices in the red-near-infrared spectral domain for burned land discrimination. **International Journal of Remote Sensing**, v. 23, n. 23, p. 5103-5110, 2002. <https://doi.org/10.1080/01431160210153129>
- COCHRANE, M. A. Fire science for rainforests. **Nature**, v. 421, p. 913-919, 2003.. <https://doi.org/10.1038/nature01437>
- DODONOV, P. Air and soil temperature across fire-created edges in a Neotropical rainforest. **Agricultural and Forest Meteorology**, v. 276-277, 2019. <https://doi.org/10.1016/j.agrformet.2019.06.005>
- DOS SANTOS, J. F. C., et al. Potentials and limitations of remote fire monitoring in protected areas. **Science of the Total Environment**, v. 616-617, p. 1347-1355, 2018. <https://doi.org/10.1016/j.scitotenv.2017.10.182>
- DURRIEU, S. et al. Influence of training sampling protocol and of feature space optimization methods on supervised classification results. 2007. **IEEE International Geoscience and Remote Sensing Symposium**, Barcelona, p. 2030-2033, 2007. <https://doi.org/10.1109/IGARSS.2007.4423229>
- DEFINIENS. **Developer XD 2.0.4: reference book**. Munique: DEFINIENS, 2012, 414 p.
- DEMPWOLF, J., et al. Burned-Area mapping of the serengeti-mara region using MODIS reflectance data. **IEEE Geoscience and Remote Sensing Letters**, v. 4, n. 2, p. 312-316, 2007. <https://doi.org/10.1109/LGRS.2007.894140>

- ESCUÍN, S.; NAVARRO, R.; FERNÁNDEZ, P. Fire severity assessment by using NBR (Normalized Burn Ratio) and NDVI (Normalized Difference Vegetation Index) derived from LANDSAT TM/ETM images. **International Journal of Remote Sensing**, v. 29, n. 4, p. 1053-1073, 2008. <https://doi.org/10.1080/01431160701281072>
- FREITAS, et al. Emissões de queimadas em ecossistemas da América do Sul. **Estudos Avançados**, vol. 19, n. 53, p. 167-185, 2005. <https://doi.org/10.1590/S0103-40142005000100011>
- GABRIEL, C. G. F. **Análise comparada de segmentação e classificação orientada por objectos de uma imagem Worldview-2**. 2013. 153 f. Dissertação (Mestrado em Gestão do território) - Universidade Nova de Lisboa, Lisboa, 2013.
- HUETE, A. R., A soil-adjusted vegetation index (SAVI). **Remote Sensing of Environment**, vol. 25, p. 295-309, 1988. [https://doi.org/10.1016/0034-4257\(88\)90106-X](https://doi.org/10.1016/0034-4257(88)90106-X)
- IBGE. **Censo Agropecuário**. 2017. Available in: <https://cidades.ibge.gov.br/brasil/ba/una/pesquisa/24/76693>. Accessed: May 26, 2020.
- IBGE. **Estimativa da população - 2019**. Available in: <https://cidades.ibge.gov.br/brasil/ba/una/panorama>. Accessed: May 26, 2020.
- INMET. **BDMEP - Banco de dados meteorológicos para ensino e pesquisa**. Available in: <http://www.inmet.gov.br/portal/index.php?r=bdmep/bdmep>. Accessed: May 26, 2020.
- INPE - Instituto Nacional de Pesquisas Espaciais. Banco de dados de queimadas. 2018. Available in: <http://queimadas.dgi.inpe.br/queimadas/bdq ueimadas>. Accessed: March 22, 2018.
- JENSEN, J.R. **Sensoriamento remoto do ambiente: uma perspectiva em recursos terrestres**. São José dos Campos: Parêntese, 2009. p 357-410
- KEY, C. H.; BENSON, N. C. **The Normalized Burn Ratio (NBR): A Landsat TM radiometric measure of burn severity**. US Dept. Interior, Northern Rocky Mountain Sci. Center, Bozeman, MT. 1999.
- LANDIS, J.R.; KOCH, G.G. The measurement of observer agreement for categorical data. **Biometrics**, vol. 33, n. 1, 1997. pp. 159-174. <https://doi.org/10.2307/2529310>
- LEDUC, F. Feature space optimization prior to fuzzy image classification. In: **Proceedings of the 7th International Conference of Information Fusion**, p. 547-554, 2004. Available in: <http://www.fusion2004.foi.se/papers/IF04-0547.pdf>. Accessed: September 15, 2018.
- LEITE, C. C. S. de S., et al. **Análise dos incêndios ocorridos no Parque Nacional da Chapada Diamantina-Bahia em 2008 e 2015 com suporte em índices espectrais de vegetação**. **Revista Brasileira de Cartografia**, v. 69, n. 6, p. 1127-1141, 2017. Available in: <http://www.seer.ufu.br/index.php/revistabrasileiracartografia/article/view/44315/23397>. Accessed: May 26, 2020.
- MAPBIOMAS. **Coleção 4.1 da Série Anual de Mapas de Cobertura e Uso de Solo do Brasil**. 2020. Available in: <https://mapbiomas.org/>. Accessed: May 28, 2020.
- MARTÍN, M. P.; GÓMEZ, I.; CHUVIECO, E. Performance of a burned-area index (BAIM) for mapping Mediterranean burned scars from MODIS data. In: RIVA, J.; PÉREZ-CABELLO, F.; CHUVIECO, E. (Eds.). **Proceedings of the 5th International Workshop on Remote Sensing and GIS applications to Forest Fire Management: Fire Effects Assessment**, Paris, p. 193-198, 2005.
- MARTÍN, M. P. I.; CHUVIECO, E. Cartografía de grandes incêndios forestales en la península ibérica a partir de imágenes NOAA-AVHRR. **Serie Geográfica**, vol. 7, p. 109-128, 1998. Available in: <https://digital.csic.es/handle/10261/6426>. Accessed: April 20, 2018.
- McDERMID, G.P. et al. Object-oriented analysis for change detection. In: **Proceedings of the 25th Canadian symposium on remote sensing**, 14-17 October 2003, Montreal, Canada. Available in: https://www.researchgate.net/publication/237810865_OBJECT_ORIENTED_ANALYSIS_FOR_CHANGE_DETECTION. Accessed: June 20, 2018.
- MENEZES, G. S. C.; CAZETTA, E.; DODONOV, P. Vegetation structure across fire edges in a Neotropical rain forest. **Forest Ecology and Management**, v. 453, 2019. <https://doi.org/10.1016/j.foreco.2019.117587>
- MISTRY, K. BIZERRIL, M. Por que é importante entender as inter-relações entre pessoas, fogo e áreas protegidas? **Biodiversidade Brasileira**, vol. 1, n. 2, p. 40-49, 2011. Available in: <https://www.icmbio.gov.br/revistaelectronica/index.php/BioBR/article/view/137>. Acesso: 20 de março de 2018.
- PEREIRA, A. A. et al. Avaliação de nove índices espectrais quanto a separabilidade entre queimadas e diferentes alvos. In: Simpósio Brasileiro de Sensoriamento Remoto, 17. **Anais...** João Pessoa, p. 3105-3112, 2015.
- PEREIRA, A. A. **Uso de geotecnologia para detecção e análise de queimadas e focos de calor em unidades de conservação no norte de Minas Gerais**. 2009. 91 f. Dissertação (Mestrado em Engenharia Florestal) - Universidade Federal de Lavras, Lavras, 2009.
- PEREIRA, J. M. C. A Comparative Evaluation of NOAA/AVHRR Vegetation Indexes for Burned

- Surface Detection and Mapping. **IEEE Transactions on Geoscience and Remote Sensing**, v. 37, n. 1, 1999. <https://doi.org/10.1109/36.739156>
- PINTO, L. P. et al. Mata Atlântica Brasileira: os desafios para conservação da biodiversidade de um hotspot mundial. In: ROCHA, C. F. D. et al. (Ed.). **Biologia da Conservação: essências**. São Carlos: RiMa, p. 69-96, 2006.
- PINTY, B.; VERSTRAETE, M. M., GEMI: A non-linear index to monitor global vegetation from satellites, **Vegetation**, v. 101, n. 1, p. 15–20, 1992. <https://doi.org/10.1007/BF00031911>
- PONZONI, F. J.; SHIMABUKURO, Y. E. **Sensoriamento remoto no estudo da vegetação**. São José dos Campos: Parêntese, 2007. 127 p.
- QI, J. et al., Modified Soil Adjusted Vegetation Index (MSAVI). **Remote Sensing of Environment**, v. 48, n. 2, p. 119-126, 1994. [https://doi.org/10.1016/0034-4257\(94\)90134-1](https://doi.org/10.1016/0034-4257(94)90134-1)
- ROSAN, T. M.; ALCÂNTARA, E. Detecção de áreas queimadas e severidade a partir do índice espectral ΔNBR. In: Simpósio Brasileiro de Sensoriamento Remoto, 17. **Anais...** João Pessoa, 2015. p. 526-533.
- ROUSE, J.W. et al. Monitoring vegetation systems in the Great Plains. **Earth Resources Technology Satellite-1 Symposium**, Washington, DC, p. 309–317, 1973.
- SANTOS, J. F.; SOARES, R. V.; BATISTA, A. C. Perfil dos incêndios florestais no Brasil em áreas protegidas no período de 1998 a 2002. **Floresta**, v. 36, n. 1, 2006. <https://doi.org/10.5380/rf.v36i1.5510>
- SANTOS, S. M. B. dos, et al. Assessment of Burned Forest Area Severity and Postfire Regrowth in Chapada Diamantina National Park (Bahia, Brazil) Using dNBR and RdNBR Spectral Indices. **Geosciences**, v.10, n. 106, 2020. <https://doi.org/10.3390/geosciences10030106>
- SAVE BRASIL; IESB; BIRDLIFE INTERNATIONAL. **Complexo de Serras das Lontras e Una, Bahia**: Elementos naturais e aspectos de sua conservação. São Paulo: SAVE Brasil, 2009. 60 f.
- SOLLBERG, I.; SCHIAVETTI, A.; MORAES, M. E. Manejo Agrícola no Refúgio de Vida Silvestre de Una: agroflorestas como uma perspectiva de conservação. **Revista Árvore**, v. 38, n. 2, p. 241-250, 2014. <https://doi.org/10.1590/S0100-67622014000200004>
- TORRES, F. T. P. Análise do perfil dos incêndios florestais no Parque Estadual da Serra do Brigadeiro e entorno (MG). **Ciência Florestal**, v. 28, n. 3, p. 1008-1021, 2018. <http://dx.doi.org/10.5902/1980509833384>
- TORRES, F. T. P. Risk mapping of fires in vegetation in the Serra do Brigadeiro State Park (MG) and surroundings. **Revista Árvore** v.41, n.2, p. 1-9, 2017. <https://doi.org/10.1590/1806-90882017000200009>
- TRIMBLE. **eCognition Developer**: user guide. Munich, Germany: Trimble Germany, Document version 9.0.1, 2014. 262 f. Available in: <www.eCognition.com>. Accessed: February 26, 2018.
- USGS. **United States Geological Survey 2018**. Available in: <<https://landsat.usgs.gov/what-are-band-designations-landsat-satellites>>. Accessed: February 22, 2018.
- VERMOTE, E., et al. Preliminary analysis of the performance of the Landsat 8/OLI land surface reflectance product. **Remote Sensing of Environment**, v. 185, nov. p. 46-56, 2016. <https://doi.org/10.1016/j.rse.2016.04.008>
- WILSON, E. H.; SADER, S. A. Detection of forest harvest type using multiple dates of Landsat TM imagery, **Remote Sensing of Environment**, v. 80, p. 385-396, 2002. [https://doi.org/10.1016/S0034-4257\(01\)00318-2](https://doi.org/10.1016/S0034-4257(01)00318-2)
- WONG, T. H., et al. (2003) Feature extraction based on object-oriented analysis. In: **Proceedings of ATC 2003 Conference**, Malaysia, 2003. Available in: <<https://www.semanticscholar.org/paper/FEATURE-EXTRACTION-BASED-ON-OBJECT-ORIENTED-WongT.-Mansor/b872d775d32c41741ee543149b983d67afaf25bb>>. Accessed: September 25, 2018.
- ZANOTTA, D. C. et al. Detecção de queimadas no Pantanal a partir de classificação orientada a objeto e informações multiespectrais de sensoriamento remoto. In: Simpósio de Geotecnologias no Pantanal, 3. **Anais...** Cáceres, p. 800-808, 2010.